https://doi.org/10.1038/s44306-025-00118-8

Rotating spin wave modes in nanoscale Möbius strips

Ashfaque Thonikkadavan[1], Massimiliano d'Aquino[2] ✉ & Riccardo Hertel[1] ✉

Curved and topologically nontrivial magnetic structures offer new pathways to control spin-wave behavior beyond planar geometries. Here, we study spin-wave dynamics in Möbius-shaped soft-magnetic nanostrips using micromagnetic simulations. By comparing single-, double-, and triple-twisted Möbius strips to a topologically trivial bent ring, we isolate the roles of helical twist and non-orientable topology. Möbius geometries exhibit non-degenerate mode doublets associated with counterpropagating spin waves, in contrast to the standing-wave doublets in the trivial case. This splitting arises from a twist-induced geometric (Berry) phase that breaks propagation symmetry, producing non-reciprocal dispersion relations. The Möbius topology further imposes antisymmetric boundary conditions, resulting in half-integer wavelength quantization. Local RF excitation allows for the selective generation of spin waves with defined frequency and propagation direction. An analytical model reproduces the dispersion behavior with excellent agreement. These results highlight how geometric and topological design can be leveraged to engineer spin-wave transport in three-dimensional magnonic systems.

The emergence of three-dimensional (3D) nanomagnetism has opened up new frontiers in the study of magnetization dynamics, extending beyond the well-charted territory of planar thin-film systems[1–3]. While magnetic thin films have been intensely investigated for decades, the ability to fabricate and probe 3D magnetic architectures[4–11] enables the exploration of physical phenomena that have no analog in planar systems, where three-dimensional geometry, topology, and curvature can profoundly modify magnetic textures and spin-wave dynamics[12–17].

Within this broader context, 3D magnonics[2,18,19] has rapidly become a vibrant research field, seeking to understand and harness spin-wave phenomena in complex 3D geometries[3]. Parallel to this, curvilinear magnetism[20], where curvature and torsion act as effective interactions, has gained growing attention for the novel magnetic textures and dynamic responses it enables.

Due to their unique geometry and topology, Möbius ring structures have attracted interest across multiple areas of physics involving transport and oscillatory phenomena, including photonics[21], quantum systems[22], phonon dynamics[23], and microwave resonators[24]. In this work, we investigate spin-wave dynamics in Möbius-shaped soft-magnetic nanostructures, which combine three-dimensionality, curvature, and nontrivial topology. Möbius strips possess a non-orientable surface and intrinsic helical twist[25], distinguishing them from topologically trivial ring structures. We use full-scale finite-element (FEM) micromagnetic simulations to model spin-wave dynamics with high accuracy in both time[26] and frequency[27] domains, to capture the effects of smooth curvature and topology on mode formation and propagation.

A central result is the helicity-dependent splitting, i.e., a lift of degeneracy, between clockwise and counterclockwise propagating modes—a phenomenon absent in topologically trivial strips, where such modes are locked into standing waves by symmetry. Furthermore, the broken symmetry in the Möbius geometry enables frequency-selective excitation of clockwise or counterclockwise rotating modes even under a linearly oscillating magnetic field, providing a simple means to access chiral spin-wave dynamics. We numerically extract the magnon dispersion relations for Möbius strips with one, two, and three twists, which, due to the quantization by the circular boundary conditions, result in a distinct set of frequencies and wave vectors. We utilize an analytical model[28] that reproduces the essential spin-wave dynamics in the Möbius strips. The theoretical predictions show excellent agreement with micromagnetic simulations. These findings highlight how topology and 3D curvature can fundamentally alter magnonic behavior, offering new strategies for engineering spin-wave transport in next-generation nanoscale devices.

Results

Previous studies on magnetic Möbius strips have focused primarily on static magnetic textures[29]. In particular, systems with perpendicular magnetic anisotropy have been shown to support topologically protected 180° Bloch-type domain walls stabilized by the strip's non-orientable geometry. Beyond

[1]Université de Strasbourg, CNRS, Institut de Physique et Chimie des Matériaux de Strasbourg, Strasbourg, France. [2]Department of Electrical Engineering and ICT, University of Naples Federico II, Naples, Italy. ✉e-mail: mdaquino@unina.it; riccardo.hertel@ipcms.unistra.fr

the static regime, analytical work has predicted how curvature and torsion can affect spin-wave propagation in curved magnetic structures, including ferromagnetic Möbius geometries[30,31] and antiferromagnetic helical wires[32]. An experimental demonstration of nanoscale Möbius-shaped magnetic rings has also been reported[8], highlighting the feasibility of such structures for future magnonic applications.

In contrast to these earlier works, we investigate dynamic spin-wave behavior in soft-magnetic Möbius strips using full-scale micromagnetic simulations. The ground state is a topologically trivial annular vortex, and it is primarily the dynamic response, rather than the static configuration, that is affected by the strip's geometric and topological features. In particular, the perpendicular components of the dynamic magnetization are influenced by the geometry and topology.

As a model system, we consider a Permalloy Möbius strip with a diameter of 100 nm, a width of 20 nm, and a thickness of 2 nm, as shown in Fig. 1a). Due to its nonzero thickness, the structure is technically orientable and topologically equivalent to a torus. However, in a micromagnetic sense, its strong shape anisotropy and minimal thickness constrain the magnetization to lie in-plane, with negligible variation across the thickness. As a result, the system behaves as an effectively two-dimensional magnetic structure, with its topological characteristics directly influencing the dynamic magnetization field.

We expect that key features of the Möbius geometry will strongly influence spin-wave dynamics, particularly for modes propagating along the strip's circumference. First, unlike a flat strip of identical width and thickness, the Möbius strip exhibits a continuous helical twist with an intrinsic handedness defined by its geometry. Second, its reconnection creates a non-orientable surface, leading to nontrivial periodic boundary conditions. In addition, the finite size of the structure results in a discrete, quantized set of resonance modes and frequencies, in contrast to extended planar strips. As we will show later, these geometric and topological features produce distinct effects, including the emergence of geometric phases in the spin-wave modes. By contrast, the circular curvature introduced by closing the strip into a ring plays only a minor role.

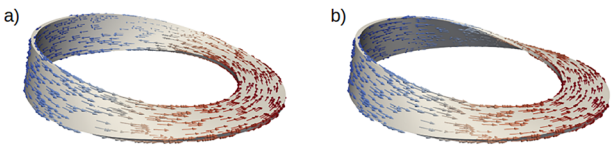

Fig. 1 | Soft-magnetic annular nanostrips with identical material, geometric parameters (thickness, radius, and width), but differing topology. a The Möbius strip features a non-orientable surface with constant torsion along the circumference. **b** The twist-compensated "bent" ring is topologically trivial and has a similar local torsion, but with alternating handedness. In both cases, the equilibrium magnetic state is a macroscopic vortex configuration, with the magnetization closely aligned along the tangential direction. Spin waves propagating along the strips experience antisymmetric boundary conditions in the Möbius strip (**a**) and ordinary, symmetric boundary conditions in the bent ring (**b**).

To isolate the effects of twist and topology, we compare the Möbius strip to a control structure with the same material properties and geometric parameters (thickness, width, and radius), but differing in topology, as shown in Fig. 1b. Specifically, we consider a topologically trivial "bent" ring —similar in spirit to the photonic system studied by Wang et al.[21]—in which the strip is twisted so that its local surface is perpendicular to the ring plane on one side and parallel on the opposite side. This twist-compensated ring closely matches the Möbius strip in local curvature over most of its length, but consists of two semicircular segments with opposite helicity and no net topological twist.

This comparison allows us to disentangle the individual roles of curvature, local twist, and global topology in shaping spin-wave behavior. For brevity, we limit the discussion to the case of a left-handed Möbius strip; the right-handed version yields analogous, mirror-symmetric results. In both geometries, the equilibrium magnetic configuration (in the absence of external fields) is an annular vortex, with the magnetization lying in-plane and closely following the local tangential direction of the twisted strip.

Resonant modes

We begin by analyzing the spin wave dynamics in the case of the bent, twist-compensated ring. To characterize its intrinsic high-frequency properties, we compute the first 30 eigenmodes, covering a frequency range up to approximately 45 GHz. Since our primary interest lies in understanding how twist and topology influence spin-wave behavior, considering only the first few modes is sufficient to analyze the system's magnonic properties. These modes exhibit well-defined azimuthal spin-wave patterns in the regime below about 20 GHz. In contrast, at higher frequencies, the mode patterns become increasingly complex as radial standing-wave patterns occur, with wavelengths comparable to the strip width.

We observe distinct standing-wave patterns characterized by a growing number of nodes and antinodes with increasing mode frequency. These results reflect the quantization of spin-wave modes due to the finite ring circumference and its periodic boundary conditions. While such spin-wave quantization corresponds to what is expected in flat, planar magnetic rings[33], we notice the appearance of frequency doublets, each corresponding to a pair of modes with the same number of nodes and antinodes, but different wave profiles, see Fig. 3a). The modified geometry of the bent ring leads to the appearance of mode doublets—pairs of nearly degenerate frequencies. This effect arises from the azimuthal asymmetry introduced by the bend, causing the nodes and antinodes to localize at well-defined regions of the ring. Specifically, the modes develop either maxima or minima in the area where the strip stands perpendicular or parallel to the ring plane (the inflection points of the torsion), leading to a two-fold appearance of modes of the same order.

The lowest-frequency mode, at 8.60 GHz (not shown in Fig. 2), is the FMR mode in which the entire sample oscillates in phase. While the phase of

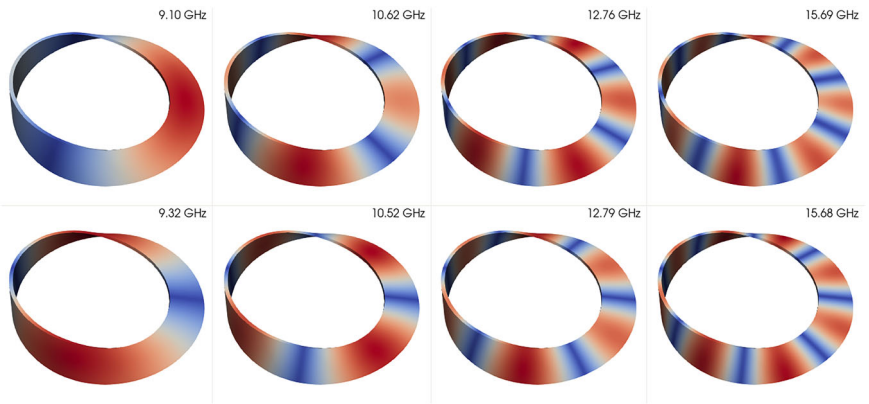

Fig. 2 | The first eight standing-wave modes in the bent, twist-compensated ring. The color code indicates the oscillation amplitude, namely the amplitude of the dynamic magnetization field $\delta \boldsymbol{m}$ (see "Methods"), rescaled for each panel, with blue indicating regions of lowest amplitudes (nodes) and red regions of maximum activity (antinodes). The lowest-frequency FMR-type mode (8.60 GHz), which exhibits oscillations of uniform phase, without a standing-wave character, is not shown.

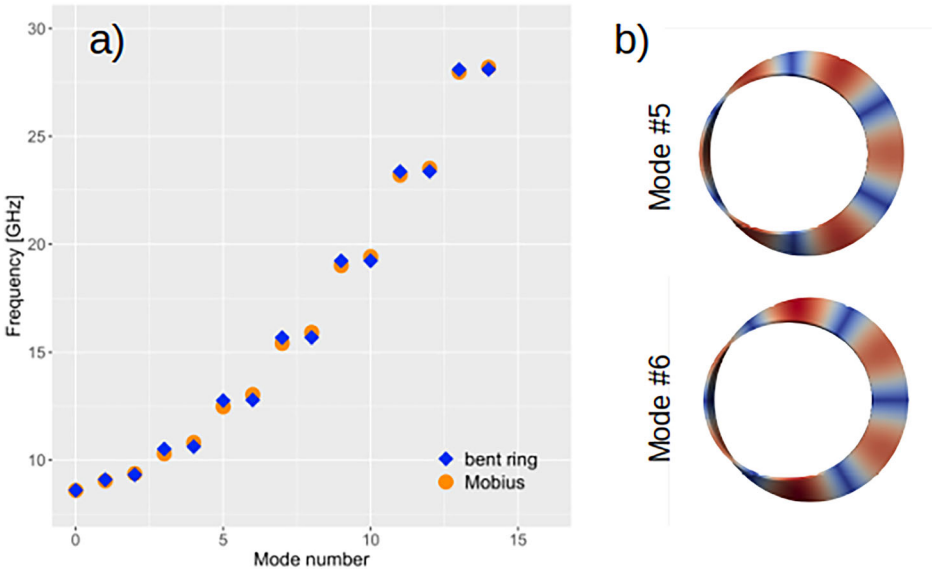

Fig. 3 | Frequency doublets of eigenmodes in the bent ring. a Eigenmode frequencies as a function of mode number, starting from the lowest-frequency mode. Except for the zero-frequency mode (the ferromagnetic resonance, FMR), all modes appear as nearly degenerate pairs—frequency doublets. A similar pattern is observed in the Möbius strip. **b** Spatial profiles of an example doublet: mode #5 and mode #6. Both modes have the same wavelength and identical numbers of nodes and antinodes, but differ in the spatial positioning of their nodes and antinodes, which are shifted relative to each other along the ring. Color indicates the oscillation amplitude, with red corresponding to antinodes (maximum amplitude) and blue to nodes (minimum amplitude).

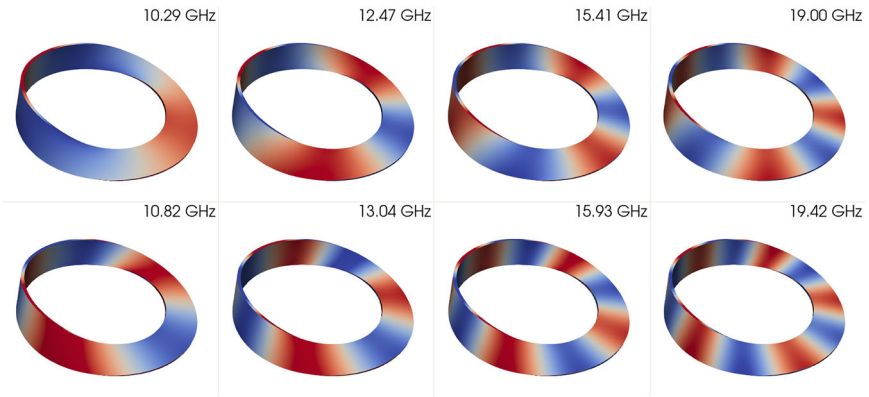

Fig. 4 | Spin-wave eigenmodes in the Möbius strip. Modes #3 through #10 are shown, with each column representing a pair of modes with similar frequency (doublets). The top row shows modes propagating counterclockwise; the bottom row shows the corresponding clockwise-propagating modes. Each image displays the mode profile at a single phase in time. Color indicates the projection of the dynamic magnetization field $\delta \boldsymbol{m}$ (see "Methods") onto the local surface normal. In each panel, the color scale is normalized independently to its minimum and maximum values.

the oscillation is homogeneous, the oscillation amplitude varies significantly across the ring, with a clear maximum localized in the perpendicularly bent region. The following two modes, at 9.10 GHz and 9.32 GHz, are long-wavelength standing modes whose profile is not well-defined, as their wavelength corresponds to the ring's perimeter. Their wave profiles are difficult to interpret unambiguously as they are significantly affected by the strip's torsion, with the wave undergoing substantial changes in surface orientation over its wavelength. Nevertheless, upon close inspection, one sees that these modes represent a doublet, with one having a maximum oscillation in the perpendicular and horizontal regions and the other exhibiting maximum oscillation in the twisted branches. All subsequent modes are clearly recognizable as doublets of standing-wave patterns with an even number of (anti-)nodes. In Fig. 2, the mode doublets are grouped columnwise, with the row at the top displaying the modes where the horizontal segment on the right is an antinode. The bottom row shows the modes complementary to those of the top row, in which that region is a node.

A similar appearance of frequency doublets is also observed in the eigenmodes of the Möbius strip, as shown in Fig. 3a). In this case, too, the lowest-frequency mode is an FMR-type oscillation of uniform phase at 8.60 GHz with a frequency nearly identical to that of the bent ring. Similar to the bent ring, the two next-higher frequency modes don't display a clear wave pattern, as the magnetic modulation occurs on a length scale corresponding to the ring's circumference. At higher frequencies, however, the mode character becomes clearly discernible and changes qualitatively compared to the topologically trivial ring: the standing-wave patterns are replaced by propagating modes. While these modes also form doublets, the lifted degeneracy now reflects the direction of propagation—clockwise or counterclockwise around the Möbius strip, with one circulation direction consistently showing a slightly higher frequency than the other, see Fig. 4. The modes' sense of rotation alternates strictly in the sequence of modes, revealing an apparent helicity-dependent symmetry breaking absent in the topologically trivial ring.

Unlike the nearly degenerate mode doublets observed in the bent ring, the spin-wave modes in the Möbius strip appear in closely spaced pairs but with clearly distinct frequencies, cf. Fig. 5a). To understand this frequency splitting, it is helpful to consider the standing-wave modes in the bent ring as superpositions of two counterpropagating spin waves with identical frequency and wavelength. The resulting mode profiles differ only in their phase, i.e., in the positioning of nodes and antinodes around the ring —leading to mode doublets with nominally identical eigenfrequencies.

In the Möbius strip, this degeneracy is lifted, resulting in pairs of eigenmodes with clearly separated frequencies. The formation of frequency doublets has been predicted in the literature in the case of planar magnetic nanorings with vortex configurations under perpendicular magnetic fields, where the splitting arises from field-induced symmetry breaking[34]. In contrast, the origin of the splitting in our case lies in the geometry: the continuous twist of the strip introduces a geometric phase[35] (a Berry phase[36] or Hannay angle[37]) that accumulates as the spin wave propagates along the structure. This geometric phase depends on the helicity of the strip and

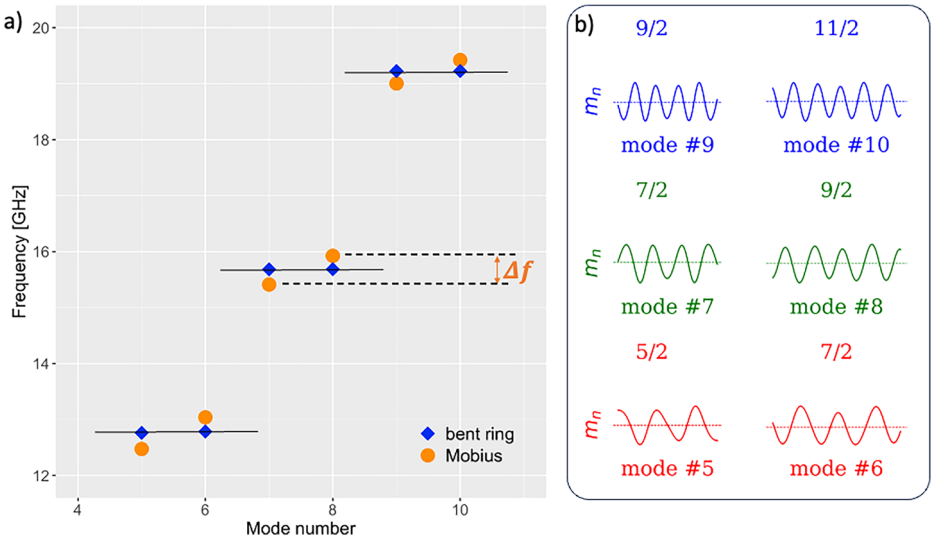

Fig. 5 | Frequency splitting of spin-wave mode doublets in the Möbius strip. a Mode frequencies for the Möbius strip (orange circles) and the bent ring (blue diamonds). While the bent ring exhibits nearly degenerate doublets, the Möbius strip shows a clear frequency splitting. For example, modes #7 and #8 in the bent ring both resonate at 15.68 GHz, whereas the corresponding Möbius modes occur at 15.41 GHz and 15.93 GHz, yielding a frequency difference of $\Delta f \approx 520$ MHz. **b** Line scans of the dynamic magnetization projected along the central path of the Möbius strip, shown for several modes. The numbers above each scan indicate the number of wavelengths (in units of 2π phase) along the circular path. The scans exhibit odd half-integer mode numbers, consistent with the antisymmetric boundary conditions imposed by the Möbius topology. Clockwise and counterclockwise modes display visibly different wavelengths.

changes sign with the propagation direction. As a consequence, clockwise and counterclockwise spin waves experience different phase shifts over one complete circuit, which in turn modifies their effective wavelengths. Since the frequency of a spin-wave mode depends on its wavelength, this asymmetry lifts the degeneracy between the two propagation directions, resulting in the observed frequency splitting within each mode pair. As a result of this frequency splitting, a standing-wave mode, formed by the superposition of two counterpropagating waves of identical wavelength and frequency, is no longer possible in the Möbius strip.

In addition to the twist-induced Berry phase, spin-wave modes in the Möbius strip are constrained by quantization due to its non-orientable surface, which imposes antisymmetric boundary conditions. These conditions require the dynamic magnetization to change sign after one full circuit, leading to quantized modes with half-integer numbers of wavelengths along the strip's circumference. Figure 5b shows line scans of the dynamic magnetization component projected onto the local surface normal, taken along the strip's central path. The scans reveal clear differences in wavelength between clockwise and counterclockwise modes within each doublet and confirm the appearance of odd-numbered half-integer wavelength modes, consistent with the Möbius geometry.

To disentangle the effects of topology-induced boundary conditions from those of the geometric phase introduced by the strip's helical twist, we extended the analysis to double- and triple-twisted Möbius geometries. The twist of each strip can be quantified by its torsion τ, which measures the continuous rotation of the local reference frame along the closed centerline of the strip. In the single-twisted Möbius strip, the local frame rotates by a total angle of π over the circumference L, yielding $\tau = \pi/L$. The double-twisted strip has $\tau = 2\pi/L$, the triple-twisted one $\tau = 3\pi/L$, while the bent ring —whose two halves carry opposite twists—has zero net torsion ($\tau = 0$). The torsion thus serves as a convenient parameter characterizing the overall geometric twist of the strip. As shown below, the presence of a finite net τ leads to a frequency splitting between counterpropagating spin-wave modes. The magnitude of this splitting increases with $|\tau|$, whereas structures with $\tau = 0$ display reciprocal spectra. Reversing the sign of τ inverts the sense of non-reciprocity.

The simulations show that circulating spin-wave modes also emerge in double- and triple-twisted Möbius structures, with only minor qualitative differences compared to the single-twist strip. As before, clockwise and counterclockwise propagating modes appear as doublets; however, the frequency splitting between them increases slightly with the number of twists. This trend suggests that the emergence of circulating modes is not dictated by the boundary conditions associated with non-orientability—which are restored to symmetry in the double-twist case—but rather by the presence and degree of helical twist in the strip geometry.

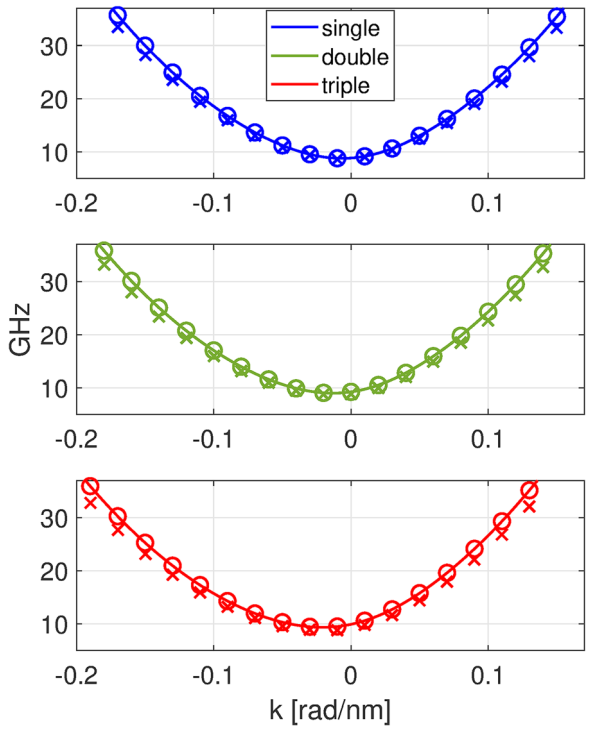

Fig. 6 | Comparison between theory and 3D FEM numerical results for single-, double-, and triple-twisted Möbius strips. Solid lines refer to the analytical dispersion relation (1), open circles indicate the discrete k-values from the quantization rule (3), and crosses denote FEM simulation results.

Dispersion relations

We simulated the dispersion relations of circulating spin-wave modes in single-, double-, and triple-twisted Möbius strips by numerically extracting the wave vector for each eigenmode. This analysis allows us to relate spin wave length and frequency and thereby to quantify how the geometry and twist affect spin-wave propagation.

The resulting dispersion relations, shown as cross symbols in Fig. 6, exhibit clear non-reciprocal behavior, with $\omega(k) \neq \omega(-k)$. This observation

Table 1 | Comparison between simulated and analytic results for the first six modes in the simple, double-, and triple-twisted Möbius geometries

Mode	single		double		triple	
number	*f*	*k*	*f*	*k*	*f*	*k*
0	8.60	−9.99	8.79	−19.98	8.83	−9.99
	8.78	−10.00	9.07	−20.00	9.52	−10.00
1	9.04	10.06	8.85	0.00	8.92	−29.97
	9.15	10.00	9.25	0.00	9.47	−30.00
2	9.38	−29.95	9.52	−39.96	9.59	−49.93
	9.52	−30.00	9.91	−40.00	10.34	−50.00
3	10.29	30.00	10.00	19.98	9.82	10.00
	10.61	30.00	10.53	20.00	10.61	10.00
4	10.82	−49.94	11.00	−59.94	11.13	−69.93
	11.20	−50.00	11.59	−60.00	11.98	−70.00
5	12.47	49.97	12.05	39.96	11.67	29.97
	13.02	50.00	12.82	40.00	12.75	30.00

Frequencies *f* are given in GHz and wave vectors *k* in rad μm^{-1}. For each mode, the simulated values are listed in the first row, and the corresponding analytical values are displayed directly below.

is consistent with previous analytical work on curved magnetic nanostrips[30,31], which predicted non-reciprocal spin wave propagation due to geometric effects. The dispersion curves display a distinct asymmetry, including off-centered minima that do not occur at $k = 0$. Here, positive and negative wavevectors correspond to clockwise and counterclockwise propagation, respectively. As the number of twists increases—from the single to the double- and triple-twisted Möbius strips—the asymmetry in the dispersion becomes more pronounced. This trend is consistent with the twist-induced geometric phase discussed earlier, which breaks the degeneracy between propagation directions and modifies the effective wavelength.

In order to provide further interpretation of the finite element calculations, we compare them with analytical formulas for spin wave dispersion relations in twisted nanostrips. The nanostrips have rectangular cross sections with thickness d comparable to the exchange length ℓ_{ex} of the material, their length L is much larger than the width w, and the axis curve (middle line) has constant curvature κ and torsion τ.

The latter assumptions imply that the magnetization profile exhibits no change along the thickness and weak variation along the width, which means that the spatial dependence occurs mainly along the axis having a curvilinear abscissa $u \in [0, L]$. When the equilibrium magnetization is quasi-tangential to the strip axis, the spin wave oscillations at each abscissa u will occur in the plane $(\boldsymbol{e}_1(u), \boldsymbol{e}_2(u))$ defined by the axis (in-plane) normal and (out-of-plane) binormal, respectively. Moreover, the small thickness $d \sim \ell_{ex}$ allows for treating magnetostatics in local form[38], which allows for introducing demagnetizing factors N_1, N_2 for the rectangular cross section[39].

A comprehensive analysis of spin wave propagation in twisted nanostrips (also including nutation due to magnetic inertia) has been performed in ref.[28]. The analytical formulas for spin wave dispersion relations relevant to the present work are readily obtained by neglecting inertial effects:

$$\begin{aligned} \omega_{\pm}(k) &= -2k\tau\ell_{ex}^2 \pm \sqrt{\omega_1(k)\omega_2(k)} \\ \omega_1(k) &= h_0 + N_1 + \ell_{ex}^2(k^2 + \tau^2 + \kappa^2), \\ \omega_2(k) &= h_0 + N_2 + \ell_{ex}^2(k^2 + \tau^2), \end{aligned} \tag{1}$$

where k is the spin wave wavenumber and h_0 is the internal effective field at equilibrium along the strip axis.

It is apparent that the presence of a nonzero torsion τ produces a symmetry breaking that reflects into the non-reciprocal spin wave propagation and the asymmetric dispersion curve[30,32], while the curvature κ only produces a positive spectral shift in the frequency response.

Moreover, it is possible to show[28] that the spin wave propagation along the nanostrip produces at the abscissa u a geometric (Berry) phase accumulation $\theta(u)$ that arises from a continuous rotation of the spin-wave polarization plane $(\boldsymbol{e}_1(u), \boldsymbol{e}_2(u))$ directly connected with the torsion:

$$\theta(u) = \int_0^u \tau(u')du' + C, \tag{2}$$

with C being an arbitrary constant phase shift. The chirality of the strip expressed by the sign of the torsion τ is responsible for the aforementioned lifted degeneracy of the spin wave doublets propagating in opposite directions.

The nontrivial topology of the Möbius strip with curvature $\kappa = 1/R$ (R is the radius of the strip axis circle) and torsion $\tau = n/(2R)$ ($n \in \mathbb{Z}$, the sign positive/negative implies right/left-handed chirality) induces a special quantization of the wavenumber due to anti-periodic boundary conditions[28] that results in the following rule:

$$k_h = \frac{n + 2h}{2R} \quad , \quad h \in \mathbb{Z}\,. \tag{3}$$

The dispersion curves for single, double, and triple (i.e. $n = -1, -2, -3$ left-handed Möbius strips) are reported in Fig. 6. The excellent agreement with the theory is apparent both concerning the non-reciprocal character of the spin wave propagation and the quantization rule (3) for wavenumbers induced by the nontrivial topology of the Möbius strips (see the open circles and "cross" symbols in Fig. 6).

To provide a quantitative comparison between the simulated data and the results obtained through the analytic formulas (1) (the internal field at equilibrium is $h_0 = -\kappa^2\ell_{ex}^2$), Table 1 lists the frequencies and the corresponding wave vectors of the first six modes for the three variants of Möbius strips.

Forced oscillations

While the eigenmode analysis reveals the system's intrinsic high-frequency characteristics, a more experimentally relevant scenario involves the response to an external oscillating field. In such cases, a high-frequency (RF) field induces forced, steady-state oscillations, leading to characteristic absorption peaks at resonant frequencies.

Figure 7 shows the RF absorption spectra for the single-, double-, and triple-twisted Möbius strips. All three geometries exhibit a prominent resonance near 9 GHz, with only minor shifts in frequency. This main absorption peak corresponds to the lowest-frequency eigenmode, located at 8.60 GHz, 8.79 GHz, and 8.82 GHz for the single-, double-, and triple-twisted cases, respectively. This mode behaves as a ferromagnetic resonance (FMR), with the magnetization oscillating in phase across the entire structure, though with strongly inhomogeneous amplitude. The largest oscillation amplitudes occur in regions where the strip width is aligned along the z axis. Because this mode lacks propagating character and involves uniform phase oscillation, the geometric and topological differences between the structures have little effect on its dynamics, resulting in nearly identical FMR responses across all three Möbius variants.

In addition to the principal FMR peak, the double- and triple-twisted Möbius strips exhibit secondary resonance peaks at 9.9 GHz and 11.67 GHz, respectively. In the double-twisted case, this secondary peak corresponds to a propagating spin-wave mode (eigenmode #3, labeled as 2 in Fig. 7) whose profile shows in-phase oscillations in the two high-susceptibility regions —where the strip width is aligned along the z axis. A similar situation arises in the triple-twisted Möbius strip, which features three such areas. There, mode #5 (labeled as 3 in Fig. 7) represents a propagating wave whose wavelength allows constructive, in-phase oscillations across all three high-susceptibility zones. These resonances illustrate how the geometry selectively enhances modes that match the spatial distribution of magnetic susceptibility.

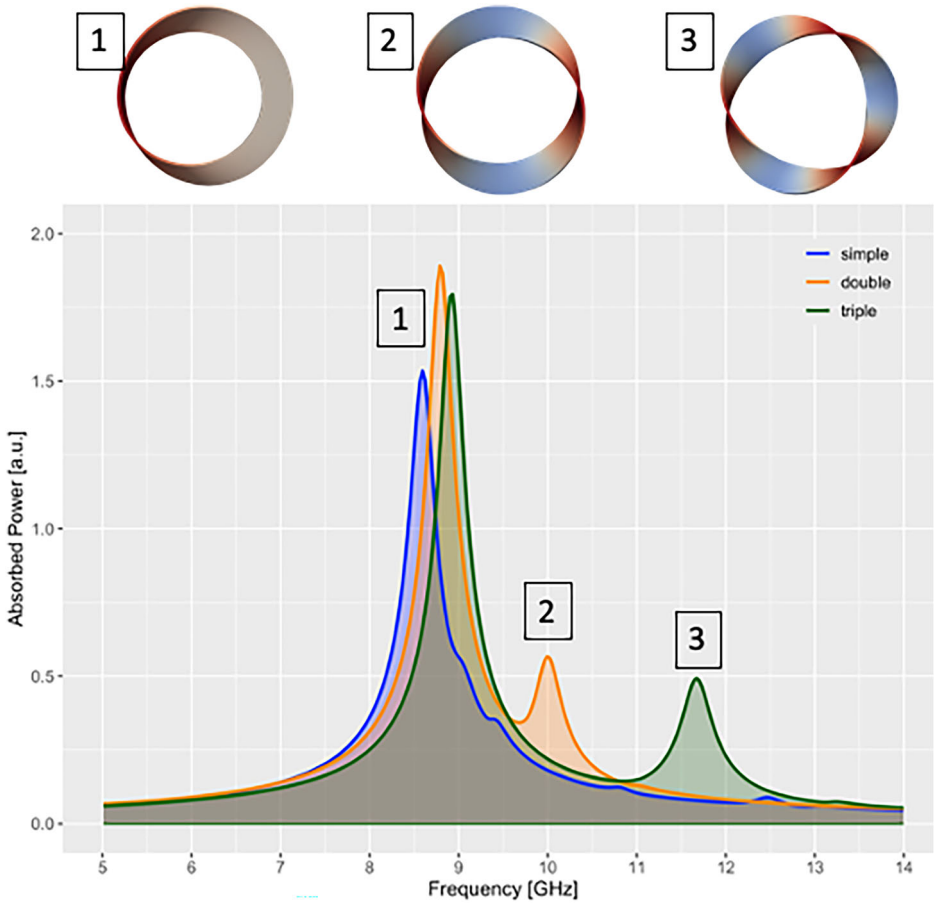

Fig. 7 | Absorption spectra of the single-, double-, and triple-twisted Möbius strips under an externally applied oscillating magnetic field. The frequency range is chosen to highlight the dominant resonance peaks. The RF field is applied perpendicular to the ring plane (along the z axis). The top panels show the dynamic magnetization profiles corresponding to the labeled peaks 1, 2, and 3 in the spectra below. Color indicates the z component of the dynamic magnetization $\delta \boldsymbol{m}$, and the snapshots are taken at the phase where the average z-component $\langle \delta m_z \rangle$ reaches its maximum.

However, aside from these geometry-matched cases, a globally applied RF field with uniform phase is generally ineffective at exciting the well-defined propagating spin-wave modes discussed in "Resonant modes". To selectively excite such modes, we apply a localized RF field restricted to a specific region of the strip. This approach allows individual eigenmodes to be excited by tuning the driving frequency to match their resonance. An example of this mode-selective excitation is shown in Fig. 8, which presents the absorption spectra of the Möbius strip and the bent ring under time-harmonic excitation localized in the high-susceptibility region—where the strip is oriented such that its width lies along the z axis.

In the topologically trivial bent ring, we observe sharp resonance peaks at well-defined frequencies, each corresponding to one of the nearly degenerate standing-wave mode doublets. Because the excitation is spatially localized, only a subset of modes is activated, specifically those for which the field is applied at or near an oscillation antinode. In our example, these correspond to the bottom row of modes shown in Fig. 2. In contrast, the Möbius strips exhibit resonance doublets with closely spaced frequencies, consistent with the eigenmode structure discussed in "Resonant modes", where each doublet corresponds to a pair of counterpropagating spin-wave modes. The use of a localized, linearly polarized RF field thus enables the excitation of spin waves with well-defined frequency and propagation direction, effectively selecting between clockwise and counter-clockwise modes.

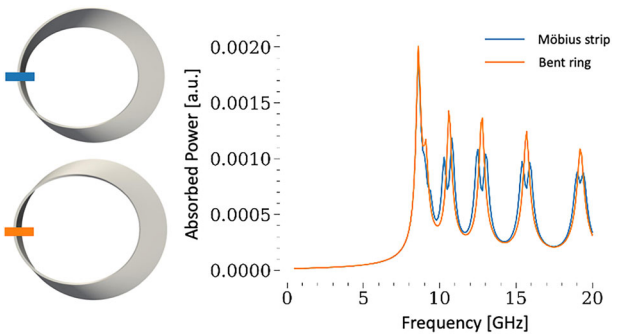

Fig. 8 | Absorption spectra of the Möbius strip and the bent ring under localized RF excitation. The excitation field is applied to a small, high-susceptibility region in each structure, as indicated by the colored rectangles in the schematics on the left (blue for the Möbius strip, orange for the bent ring). In both cases, the RF field is oriented along the z axis, perpendicular to the ring plane. The bent ring exhibits single-peak resonances at well-defined frequencies. In contrast, the Möbius strip displays double-peak structures with closely spaced frequencies, reflecting the non-degenerate nature of the counterpropagating spin-wave modes.

Discussion

Our results demonstrate how geometric twist and nontrivial topology fundamentally alter spin-wave dynamics in three-dimensional magnetic nanostructures. Using Möbius-shaped soft-magnetic strips, we show that the interplay between helical curvature and non-orientable topology leads to symmetry breaking in spin-wave propagation. In contrast to the topologically trivial bent ring, which supports degenerate standing-wave modes, Möbius strips exhibit frequency-split doublets corresponding to counter-propagating spin-wave modes. The lifting of degeneracy and the frequency-selective excitation of these modes under a linearly polarized drive illustrate how torsion-induced symmetry breaking in Möbius nanomagnets can qualitatively alter magnonic spectra. The non-reciprocity originates from a Berry phase determined by the total torsion. Although the samples studied in this work are highly regular in shape, the observed non-reciprocal effects are expected to be robust under smooth deformations that preserve the topology and overall perimeter of the strip.

While the Möbius strip is non-orientable, we find that it is not this topological feature that drives the symmetry-breaking effect, but rather the presence of a net geometric twist along the propagation path. The bent ring, though curved, features twist-compensation between its two halves, resulting in an effective zero net twist and, correspondingly, no Berry-phase-induced splitting. In the Möbius geometries, the continuous helical twist introduces a geometric (Berry) phase that modifies the effective wavelength depending on direction, breaking propagation symmetry and lifting the degeneracy between clockwise and counterclockwise modes. As a result, the Möbius strips support directionally selective, non-reciprocal spin-wave modes that cannot form standing waves. These effects grow more pronounced with increasing twist, as confirmed by our analysis of double- and triple-twisted Möbius geometries. The non-orientable topology of the Möbius strip imposes antisymmetric boundary conditions, which result in half-integer wavelength quantization. Spatially localized RF excitation enables controlled excitation of specific eigenmodes and selection of propagation direction—a mechanism that could be extended to programmable magnonic routing or phase-encoded information transfer.

Our analytical model, which closely matches the numerical dispersion data, provides a predictive framework for designing twisted magnonic systems and interpreting their spectral features. In our formulation, both curvature κ and torsion τ enter the spin-wave dispersion. The curvature κ primarily shifts the absolute resonance frequencies through local exchange fields, whereas the torsion τ governs the asymmetry between counter-propagating modes and thus gives rise to the observed non-reciprocity.

These findings highlight how geometric curvature and topological features can be harnessed to engineer magnonic responses in three-dimensional systems. The torsion-induced non-reciprocity of spin-wave propagation discussed here is, from a phenomenological standpoint, reminiscent of the asymmetry generated by intrinsic Dzyaloshinskii-Moriya interaction (DMI)[40]. Although the analytical form derived in this work does not contain an explicit DMI-type term, the observed spectral asymmetry can be interpreted as a curvature-induced effective chiral symmetry breaking, whose strength is tunable through the system's geometric parameters. Indeed, curvature-induced DMI-type effects are known to include torsional contributions[17]. Future studies may therefore explore how geometric twist and intrinsic DMI[41] jointly influence spin-wave spectra.

Methods

Mesh generation and static magnetization structure

Three-dimensional models of the Möbius-type geometries and the bent ring were generated using the open-source software FreeCAD[42]. All geometries were generated parametrically to ensure uniform curvature and torsion along the centerline, except for the bent ring, where the torsion changes sign at the symmetry axis. This procedure, which preserves a constant perimeter L for the different geometric variants, allows systematic variation of the number of twists, corresponding to torsion values of $\tau = n\pi/L$ for $n = 0, 1, 2, 3$. Tetrahedral finite-element meshes were produced with NETGEN[43], using a target cell size of 1 nm. This discretization resulted in problem sizes of slightly more than 50,000 elements for each geometry. The zero-field static magnetization configurations were computed with our GPU-accelerated open-source code `tetmag`[26]. We used Permalloy material parameters with exchange constant $A = 13$ pJ m^{-1} and spontaneous magnetization $M_s = 800$ kA m^{-1} (the exchange length is $\ell_{\mathrm{ex}} = \sqrt{2A/(\mu_0 M_s^2)} = 5.69$ nm), and vanishing magnetocrystalline anisotropy, $K_u = 0$ J m^{-3}.

Eigenmodes and forced oscillations

Eigenmodes were computed using a dedicated algorithm described in Ref.[27], which implements the formalism originally developed by d'Aquino et al.[44]. The method is based on a linearized form of the Landau-Lifshitz-Gilbert equation. Initially designed for the calculation of eigenmodes, the approach was later generalized[27] to solve micromagnetic problems involving stationary magnetic oscillations in an applied RF field.

In both situations, the method provides numerical calculation of the dynamic component of the magnetization $\delta\boldsymbol{m}(\boldsymbol{x}, t) = \boldsymbol{m}(\boldsymbol{x}, t) - \boldsymbol{m}_0(\boldsymbol{x})$ which represents the small-angle oscillation of the magnetization around the static equilibrium configuration $\boldsymbol{m}_0$. In this perturbative framework, $\delta\boldsymbol{m}$ corresponds to the oscillatory part of the magnetization in the case of spin-wave excitation.

For the forced-oscillation calculations discussed in "Forced oscillations", we assumed a Gilbert damping constant of $\alpha = 0.01$ and an RF field amplitude of 0.5 mT.

Numerical extraction of dispersion relations

Unlike extended magnetic waveguides, Möbius-type geometries form closed loops, which prevents the direct application of standard techniques for extracting dispersion relations. To address this, we map the three-dimensional eigenmode profiles onto an effective one-dimensional coordinate that traces the central path of the strip. This procedure conceptually "unrolls" the Möbius geometry into a helical waveguide, rendering it amenable to spatial Fourier analysis. By performing a Fourier transform of the dynamic magnetization $\delta\boldsymbol{m}(\boldsymbol{x}, t)$ along this path, we identify the dominant wavevectors associated with each eigenmode and thereby construct the spin-wave dispersion relation. The k-values obtained from this analysis correspond to the spin-wave wavelengths observed in the line scans shown in Fig. 5b.

Data availability

The data presented in this manuscript are available from the authors upon reasonable request.

Code availability

Our GPU-accelerated finite-element micromagnetic code, `tetmag`, which we used to calculate the static magnetic configurations, is available as open-source software[26]. In contrast, our proprietary closed-source code for simulating oscillatory magnetization dynamics in the frequency domain is not publicly available.

Received: 11 August 2025; Accepted: 31 October 2025;
Published online: 27 January 2026

References

1. Fernández-Pacheco, A. et al. Three-dimensional nanomagnetism. *Nat. Commun.* **8**, ncomms15756 (2017).
2. Gubbiotti, G. ed. *Three-Dimensional Magnonics: Layered, Micro- and Nanostructures* (Jenny Stanford Publishing, New York, 2019) https://doi.org/10.1201/9780429299155.
3. Gubbiotti, G. et al. 2025 roadmap on 3D nanomagnetism. *J. Phys.: Condens. Matter* **37**, 143502 (2025).
4. Fernández-Pacheco, A. et al. Writing 3D nanomagnets using focused electron beams. *Materials* **13**, 3774 (2020).
5. Fischer, P., Sanz-Hernández, D., Streubel, R. & Fernández-Pacheco, A. Launching a new dimension with 3D magnetic nanostructures. *APL Mater.* **8**, 010701 (2020).
6. Donnelly, C. et al. Element-specific X-Ray Phase Tomography of 3D structures at the nanoscale. *Phys. Rev. Lett.* **114**, 115501 (2015).
7. Sanz-Hernández, D. et al. Artificial Double-Helix for geometrical control of magnetic chirality. *ACS Nano* **14**, 8084 (2020).
8. Skoric, L. et al. Layer-by-layer growth of complex-shaped three-dimensional nanostructures with focused electron beams. *Nano Lett.* **20**, 184 (2020).
9. Williams, G. et al. Two-photon lithography for 3D magnetic nanostructure fabrication. *Nano Res.* **11**, 845 (2018).
10. Keller, L. et al. Direct-write of free-form building blocks for artificial magnetic 3D lattices. *Sci. Rep.* **8**, 6160 (2018).
11. Teresa, J. M. D. et al. Review of magnetic nanostructures grown by focused electron beam induced deposition (FEBID). *J. Phys. D: Appl. Phys.* **49**, 243003 (2016).
12. Hertel, R. Curvature-induced magnetochirality. *SPIN* **3**, 1340009 (2013).

13. Gaididei, Y., Kravchuk, V. P. & Sheka, D. D. Curvature effects in thin magnetic shells. *Phys. Rev. Lett.* **112**, 257203 (2014).
14. Otálora, J. A., Yan, M., Schultheiss, H., Hertel, R. & Kákay, A. Curvature-induced asymmetric spin-wave dispersion. *Phys. Rev. Lett.* **117**, 227203 (2016).
15. Streubel, R. et al. Magnetism in curved geometries. *J. Phys. D: Appl. Phys.* **49**, 363001 (2016).
16. Heyderman, L. J. et al. Mesoscopic magnetic systems: From fundamental properties to devices. *Appl. Phys. Lett.* **119**, 080401 (2021).
17. Sheka, D. D. et al. Fundamentals of curvilinear ferromagnetism: statics and dynamics of geometrically curved wires and narrow ribbons. *Small* **18**, 2105219 (2022).
18. Kruglyak, V. V., Demokritov, S. O. & Grundler, D. Magnonics. *J. Phys. D: Appl. Phys.* **43**, 264001 (2010).
19. Chumak, A. V. et al. Advances in magnetics - roadmap on spin-wave computing. *IEEE Trans. Magn.* **58**, 1 (2022).
20. Makarov, D. & Sheka, D. D. eds. Curvilinear Micromagnetism: From Fundamentals to Applications Topics in Applied Physics, Vol. 146 (Springer International Publishing, Cham, 2022) https://doi.org/10.1007/978-3-031-09086-8.
21. Wang, J. et al. Experimental observation of Berry phases in optical Möbius-strip microcavities. *Nat. Photonics* **17**, 120 (2023).
22. Flouris, K., Jimenez, M. M. & Herrmann, H. J. Curvature-induced quantum spin-Hall effect on a Möbius strip. *Phys. Rev. B* **105**, 235122 (2022).
23. Nishiguchi, N. & Wybourne, M. N. Phonon modes in a Möbius band. *J. Phys. Commun.* **2**, 085002 (2018).
24. Hamilton, J. K., Hooper, I. R. & Lawrence, C. R. Absorption modes of Möbius strip resonators. *Sci. Rep.* **11**, 9045 (2021).
25. Guo, X., Guzmán, M., Carpentier, D., Bartolo, D. & Coulais, C. Non-orientable order and non-commutative response in frustrated metamaterials. *Nature* **618**, 506 (2023).
26. Hertel, R., tetmag, https://github.com/R-Hertel/tetmag (2023)
27. d'Aquino, M. & Hertel, R. Micromagnetic frequency-domain simulation methods for magnonic systems. *J. Appl. Phys.* **133**, 033902 (2023).
28. d'Aquino, M. & Hertel, R. Nonreciprocal inertial spin-wave dynamics in twisted magnetic nanostrips (2025), arXiv:2508.05576 [cond-mat].
29. Pylypovskyi, O. V. et al. Coupling of chiralities in spin and physical spaces: The Möbius ring as a case study. *Phys. Rev. Lett.* **114**, 197204 (2015).
30. Sheka, D. D., Kravchuk, V. P., Yershov, K. V. & Gaididei, Y. Torsion-induced effects in magnetic nanowires. *Phys. Rev. B* **92**, 054417 (2015).
31. Gaididei, Y. et al. Magnetization in narrow ribbons: curvature effects. *J. Phys. A: Math. Theor.* **50**, 385401 (2017).
32. Wu, H. & Lan, J. Curvilinear manipulation of polarized spin waves. *Phys. Rev. B* **105**, 174427 (2022).
33. Zaspel, C. E. & Ivanov, B. A. Magnon modes in permalloy nanorings. *J. Magn. Magn. Mater.* **286**, 366 (2005).
34. Ivanov, B. A. & Zaspel, C. E. High frequency modes in Vortex-state nanomagnets. *Phys. Rev. Lett.* **94**, 027205 (2005).
35. Wilczek, F. & Shapere, A. *Geometric Phases in Physics | Advanced Series in Mathematical Physics*, Advanced Series in Mathematical Physics, Vol. 5 (World Scientific, 1989)
36. Berry, M. V. Classical adiabatic angles and quantal adiabatic phase. *J. Phys. A: Math. Gen.* **18**, 15 (1985).
37. Hannay, J. H. Angle variable holonomy in adiabatic excursion of an integrable Hamiltonian, *J. Phys. A: Math. Gen.* **18**, 221 (1985)
38. Gioia, G. & James, R. D. Micromagnetics of very thin films. *Proc. R. Soc. Lond. A: Math., Phys. Eng. Sci.* **453**, 213 (1997).
39. Aharoni, A. Demagnetizing factors for rectangular ferromagnetic prisms. *J. Appl. Phys.* **83**, 3432 (1998).
40. Zakeri, K. et al. Asymmetric spin-wave dispersion on Fe(110): Direct evidence of the Dzyaloshinskii-Moriya interaction. *Phys. Rev. Lett.* **104**, 137203 (2010).
41. Volkov, O. M. et al. Mesoscale Dzyaloshinskii-Moriya interaction: geometrical tailoring of the magnetochirality. *Sci. Rep.* **8**, 866 (2018).
42. Juergen, R. et al., FreeCAD: An Open-Source Parametric 3D CAD Modeler, https://www.freecad.org/ (2022), version 0.19
43. SchÖberl, J. & NETGEN Developers NETGEN: An Open-Source Finite Element Mesh Generator, https://ngsolve.org/ (2025).
44. d'Aquino, M., Serpico, C., Miano, G. & Forestiere, C. A novel formulation for the numerical computation of magnetization modes in complex micromagnetic systems. *J. Comput. Phys.* **228**, 6130 (2009).

Acknowledgements

This work was funded by the France 2030 government investment plan managed by the French National Research Agency ANR under grant reference PEPR SPIN – [SPINTHEORY] ANR-22-EXSP-0009.The authors acknowledge the High Performance Computing Center of the University of Strasbourg for supporting this work by providing access to computing resources. M.d'A. acknowledges support from the Italian Ministry of University and Research, PRIN2020 funding program, grant number 2020PY8KTC.

Author contributions

R.H. and M.d'A. conceived the research idea. R.H. wrote the main part of the manuscript. M.d'A. developed the methodology and the software implementation of the frequency-domain simulations and the analytical expression of the spin wave dispersion relation. R.H. developed the micromagnetic simulation software in the time and frequency domains (the latter in collaboration with M.d'A). A.T. and R.H. performed simulations and analyzed results. A.T. developed algorithms for the numerical analysis of the dispersion relations. All authors contributed to the writing of the manuscript, prepared figures, and participated in the discussion of the results and data analysis.

Competing interests

The authors declare no competing interests.

Additional information

Correspondence and requests for materials should be addressed to Massimiliano d'Aquino or Riccardo Hertel.